SERS From Transition Metals and Excited by Ultraviolet Light

Zhong-Qun Tian, Zhi-Lin Yang, Bin Ren, and De-Yin Wu

State Key Laboratory of Physical Chemistry of Solid Surfaces and Department of Chemistry, College of Chemistry and Chemical Engineering, Xiamen University, Xiamen, 361005, China
zqtian@xmu.edu.cn

1 Introduction

Since the mid-1990s, surface-enhanced Raman scattering (SERS) has greatly advanced and gained wider application and renewal interest than in the previous two decades [1,2,3,4,5,6,7,8,9]. There have been several new and creative developments, e.g., SERS of single molecules, nanostructures and transition metals, tip-enhanced Raman scattering (TERS), surface-enhanced hyper-Raman scattering (SEHRS), ultraviolet-excited SERS (UV-SERS), surface-enhanced resonance Raman scattering (SERRS). In this book, this Chapter is probably the only one describing metals other than Ag, Au and Cu. It may be necessary to first give a brief introduction on the development of extending SERS study to transition metals.

The major obstacle hampering the generality of SERS is that only the three coinage metals (Au, Ag, and Cu) and some alkali metals (Na [10], K [11], Li [12]) can provide the huge enhancement because they belong to free-electron metals whose surface-plasmon resonance can be efficiently excited by the visible light, and only Au, Ag and Cu can be used for practical applications. This fact severely limited the SERS application in other materials. Whereas transition metals have a much wider application in modern industries and technologies, such as electrochemistry, corrosion and catalysis, they had been commonly considered as non-SERS-active substrates by the communities of surface science and spectroscopy [13]. In fact, we do not find any SERS review articles definitely stating that transition metals exhibit SERS before 1998. In the past three decades, the development of SERS into a powerful spectroscopic tool for a wide variety of materials had been slower than expected.

However, researchers never gave up their efforts to extend SERS to the study of metallic and nonmetallic surfaces other than coinage metals [14,15,16,17,18,19,20,21,22,23,24,25,26,27,28,29,30,31,32,33,34,35,36, 37, 38, 39, 40, 41, 42, 43, 44, 45]. In the 1980s, a strategy based on "borrowing SERS" was proposed, either by depositing a SERS-active metals onto non-SERS-active substrates including semiconductors [14, 15] or by depositing non-SERS-active materials over SERS-active substrates [16,17,18,19,20,21]. For example, a SERS-active silver layer was deposited over a n-GaAS sur-

K. Kneipp, M. Moskovits, H. Kneipp (Eds.): Surface-Enhanced Raman Scattering – Physics and Applications, Topics Appl. Phys. **103**, 125–146 (2006)

face and the resonance Raman signal of dye molecules was obtained [14, 15]. Alternatively, Ni, Co, Fe, Pt, Pd, Rh and Ru ultrathin films were electrochemically deposited over SERS-active Ag or Au electrodes to obtain signals from these films. With the aid of the long-range effect of the electromagnetic (em) enhancement created by the SERS-active substrate underneath, weak SERS spectra of various adsorbates on the transition-metal overlayers have been obtained [16, 17, 18, 19, 20, 21].

It should be noted that the strong electromagnetic field generated on the SERS-active substrate will be attenuated exponentially with the increasing of thickness of the coated film so that the film has to be ultrathin, normally 3–10 atomic layers, to achieve a reasonable signal. However, it was very difficult to completely cover randomly rough substrates with such a ultrathin layer. Thus the "pinhole" in the overlayer made it extremely difficult to eliminate entirely the contribution of the giant SERS of the substrate. Weaver and coworkers made significant progress in overcoming this problem. They reported a series of work on "pinhole-free" transition metals over the SERS-active Au surface by electrochemical atomic-layer epitaxy using constant-current deposition at a low current density or by redox replacement of underpotential-deposited metals on Au [22, 23, 24, 25]. This method is very promising if one can prepare a "pinhole-free" ultrathin film of different materials with good stability in a wide range of potential or/and temperature. It makes SERS a versatile tool in studying various material surfaces of practical importance. In addition to studying the surface adsorption and reaction, the overlayer method can also be used to characterize the fine structure of the ultrathin film itself. This includes oxides, semiconductors and polymers [26, 27, 28, 29, 30]. Its advantage of high sensitivity enables one to probe ultrathin films with a few atomic monolayers.

Another totally different strategy is to generate SERS directly from transition metals [33, 34, 35, 36, 37, 38, 39, 40, 41, 42, 43, 44, 45]. There is no doubt that the surface preparation is more straightforward and the stability is higher than the substrate coated with an ultrathin film. This strategy is much more challenging as it contradicts the commonly accepted notion that transition metals were not SERS-active. This approach appeared to be the most difficult or even impossible one, and has been demonstrated since the early days of SERS. Several groups attempted to obtain unenhanced [33, 34] and enhanced [35, 36, 37, 38, 39, 40, 41] Raman signals from adsorbates on either roughened or mechanically polished Pt, In, and Rh electrodes, or porous Ni, Pd, Pt, Ti and Co films [42, 43]. In all of these studies, the reported surface spectra were obtained only under optimal conditions or by data manipulation using spectral-subtraction methods [33, 34, 35, 36]. Surface Raman signals were typically too weak to be investigated as a function of the electrode potential or temperature. In practical applications, however, such a type of measurement is quite essential. Furthermore, some results could not be repeated by other groups. The reported results were not strongly supportive of SERS studies on transition metals, and pointed to a gloomy future in

this direction. Indeed, only a few papers [38, 41, 44, 45], among many theoretical and experimental works, claimed that transition metals might have relatively weak SERS activity in comparison with the coinage metals of Au, Ag and Cu, which had not been recognized by the scientific community. As a consequence, the activity in the SERS field declined substantially from the late-1980s to the mid-1990s.

The situation has changed dramatically since the late-1990s [46, 47, 48, 49, 50, 51, 52, 53, 54] with advances in Raman instrumentation, i.e., the advent of the confocal microscope and the holographic notch filter [55, 56]. The Raman experiment, which normally employed high-dispersion double or triple monochromators to filter out the elastically scattered laser radiation, can now be performed simply with a single spectrograph together with a holographic notch filter. The throughput of a single-grating system is far higher than, for example, a triple monochromator. The optical configuration of the confocal Raman microscope was found to be very helpful for obtaining the very weak signal of the surface species without the interference of the strong signal from the bulk phase. These new developments have resulted in unprecedented sensitivity that was vitally important for making the several important advances in this field in the late-1990s.

One of the progresses is confirmation of SERS directly from many pure massive transition metals [46, 47, 48, 49, 50, 51, 52, 53, 54]. Since 1996 our group has reported our efforts to optimize the confocal Raman microscope in order to obtain the highest sensitivity, and has developed various surface-preparation procedures for different transition metals to obtain surface spectra with better signal to noise ratio. Generally, two types of substrates have often been employed in SERS studies: roughened metal electrodes and metal nanoparticle (colloid) sols. In our studies, six SERS activation procedures have been performed and/or developed for different transition metals and for different studies, i.e., potential-controlled oxidation and reduction cycle(s) (ORC) [46], current-controlled ORC [57], chemical etching [52, 53], electrodeposition [51], template synthesis [58, 59], and nanoparticles-on-electrode [60].

So far we have been able to obtain surface Raman spectra of good quality not only on the electrode surfaces made of many transition metals, such as Pt, Ni, Ru, Rh, Pd, Co, Fe and their alloys, but also over a very wide potential region (e.g., $-2.0\,\mathrm{V}$ to $+1.4\,\mathrm{V}$) [9, 13, 46, 47, 48, 49, 50, 51, 52, 53, 54]. The molecular-level investigation of diverse adsorbates at various transition-metal electrodes can be realized by Raman spectroscopy [46, 47, 48, 49, 50, 51, 52, 53, 54]. The important adsorbates already studied include CO, H, O, Cl^-, Br^-, SCN^-, CN^-, pyridine, thiourea, benzotriazole and pyrazine [46, 47, 48, 49, 50, 51, 52, 53, 54, 61, 62, 63, 64, 65]. It has been demonstrated that SERS can be widely used to study electrochemical interfaces including many transition-metal-based systems, such as electrochemical adsorption and reaction, electrocatalysis, corrosion and fuel cells [63, 64, 65, 66].

It has been found that the increase in the surface signal intensity is not simply proportional to the surface-roughness factor (R). Therefore, one should consider the existence of the SERS effect on these transition-metal surfaces. It should be pointed out that in the past about three decades, among many theoretical studies, only two papers [44, 45] claimed that transition metals might have relatively weak SERS activity in comparison with the coinage metals. In the mid-1980s *Chang* and coworkers reported a very interesting electrodynamics calculation on spheroids of Pt, Rh, Ni and Pd [44], but these important papers had not been recognized by the scientific community because transition metals were not generally considered as effective SERS substrates. Since we have already a large surface Raman signal from transition metals, it might be possible for us to clarify whether there are SERS on transition metals. We proposed a method to accurately calculate the surface-enhancement factor (G) after considering the special feature of the confocal Raman system [48, 56]. We obtained G of five roughened transition metals Fe, Co, Ni, Rh, Pd and Pt experimentally ranging from 10^2 to 10^4, in comparison with 10^6 to 10^7 for Ag, using pyridine as the probe molecule and the 632.8 nm excitation.

On the basis of the work on SERS of transition-metal surfaces, we will divide the rest of this chapter into two parts. First, we will discuss the enhancement mechanism, mainly from the physical aspect, for transition metals in comparison with the coinage metals. A three-dimensional finite difference time-domain (3D-FDTD) method was used to calculate and evaluate the local electromagnetic field that is critically dependent on the surface geometry and the size, shape and interparticle coupling of nanoparticles. Second, a new approach of using ultraviolet laser to study UV-SERS is presented, showing that the transition metals have a higher SERS activity than the coinage metals in the UV region.

2 The Physics behind SERS of Transition Metals

2.1 The Electronic Structure and Dielectric Constants of Transition Metals

Since we have successfully and systematically obtained SERS from transition metals and demonstrated that there is a SERS effect on many transition metals, it is interesting to get a clear picture of the role of the electromagnetic (em) field enhancement in the SERS of transition-metal systems. It has been well known that the em enhancement is mainly contributed by surface-plasmon resonance at geometrically defined metal nanoparticles or nanostrutures [67, 68, 69, 70, 71, 72]. The em field of the light at the surface can be greatly enhanced under conditions of collective electron resonance for "free-electron" metals classified as the coinage metals (1B group) and alkali

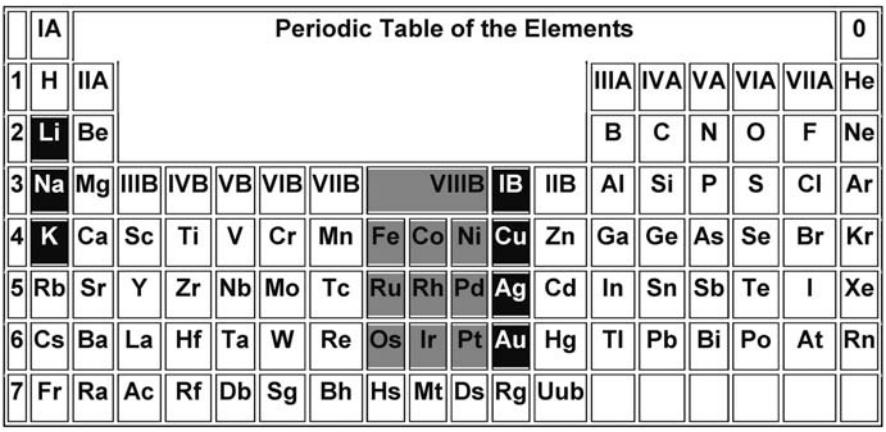

Fig. 1. A simplified periodic table of the elements. The part marked in *black* are "free-electron" metals and those marked in *gray* are transition metals

metals (1 A group) in the periodic table (see Fig. 1). In fact, all metals including transition metals can enhance the field more or less, mainly depending on the ability of metals to sustain the surface plasmon of high resonance quality. In comparison with the coinage and alkali metals, transition metals (VIIIB group) have very different electronic structures [73]. The transition metals cannot be well described by the free-electron model. The $3d$, $4d$ and $5d$ shells are always strongly mixed with the $4s$, $5s$ and $6s$ states. From the physical point of view, the Fermi level of transition metals locates at the d band. Therefore, the interband excitation occurs very possibly in the visible light region [74, 75]. The coupling between the high density of states and interband electronic transitions depresses the quality of the surface-plasmon resonance of transition metals considerably [68, 71].

To meet the conditions of good surface-plasmon resonance, the metal usually needs a small value of the imaginary component of the dielectric constant [76]. However, this is impossible for the transition metals because of their large values of the imaginary part of dielectric constants in the visible light region (see Fig. 2a). The dielectric constants in the figure are derived from the experimentally determined optical constants [77, 78] through the relationships of $\varepsilon_r = n^2 - k^2$, $\varepsilon_i = 2nk$.

Figure 2b illustrates dramatic differences in the SPR character between Pt and Ag elliptical nanoparticles with an aspect ratio of 2 : 1. The calculation is based on a two-dimensional array model proposed by *Chu* and *Wang* [79]. It can be seen that the enhancement factor of the coinage metal increases sharply when the frequency of the excitation light is close to the frequency of the surface-plasmon resonance [72, 76]. In contrast, the curves are much broader for Pt. SERS of Pt does not show any distinct character of surface-plasmon resonance, and the enhancement factors just show a slight variation

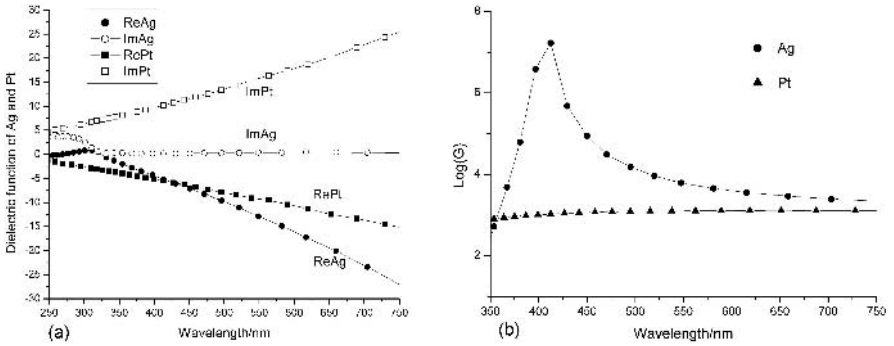

Fig. 2. (**a**) Dielectric constants of Ag and Pt; (**b**) Dependence of the surface enhancement factor (G) for two-dimensional Ag and Pt nanospheroids array on the wavelength of the incident plane wave. The semiminor axis and aspect ratio of spheroids are 20 nm and 2 : 1, respectively. The probe molecule is assumed to be located at the tip of spheroids

with the incident photon energy. This means that the SERS intensity of Pt will not vary much with the excitation wavelength in the visible light region. Our experimental results have confirmed this prediction. For instance, Pt shows almost the same SERS enhancement if we change the excitation laser from 632.8 nm (1.96 eV) to 514.5 nm (2.41 eV) while keeping all other conditions unchanged. Although the intrinsic optical property of transition metals prevents them from exhibiting intense SERS, the em enhancement still exists in the transition-metal systems with different characteristics.

2.2 Theoretical Simulation of the Local Electric Field by the Finite Difference Time-Domain Method

Several methods have been utilized to perform electrodynamics calculation of light scattering from particles of an arbitrary shape, including the finite element method (FEM), discrete dipole approximation (DDA), finite difference time-domain (FDTD) method and T-matrix method [80, 81, 82]. Among them, FDTD is a powerful tool to simulate the distribution of the electromagnetic field around the illuminated nanoparticles or substrate with an arbitrary geometry by numerically solving Maxwell's equations. Here, we will simulate the local electric field on transition-metal surfaces using the three-dimensional FDTD (3D-FDTD) method. To obtain the necessary parameters like static permittivity, infinite frequency permittivity, conductivity and the relaxation time, we fit them to the complex permittivity of metals [78] for the optical frequency range under investigation. Their relationship can be described by the general Drude model as follows [82, 83],

$$\varepsilon(\omega) = \varepsilon_\infty + \frac{\varepsilon_\mathrm{s} - \varepsilon_\infty}{1 + i\omega\tau} + \frac{\sigma}{i\omega\varepsilon_0},$$

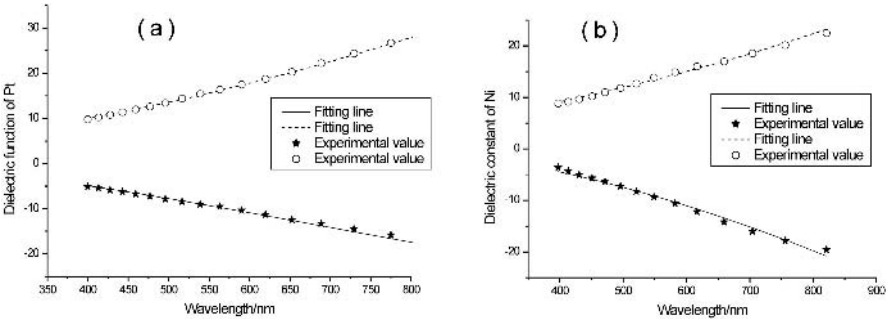

Fig. 3. Complex permittivity for Pt (**a**) and Ni (**b**) solid: *fitting line* using the general Drude model; *scatter*: experimental data

where ε_s, ε_∞, σ, τ represent the static permittivity, the infinite frequency permittivity, the conductivity and the relaxation time, respectively. ω is the angular frequency of the excitation light and ε_0 is the permittivity of free space. The four parameters ε_s, ε_∞, σ, τ can be adjusted through curve-fitting techniques to correctly match the experimental complex permittivity. Figure 3a shows a good fitting curve for the complex permittivity for platinum in the visible light region where ε_s, ε_∞, σ, τ are -62, 1, 1.18×10^6 S/m and 6.6×10^{-16} s. Similarly, a good fitting curve can be obtained for Ni with the static permittivity, the infinite frequency permittivity, the conductivity and the relaxation time of -315, 1, 2.1×10^6 S/m, and 1.6×10^{-15} s, respectively (see Fig. 3b). A more detailed description of the theoretical treatment will be given elsewhere [60].

Based on the previous theoretical works [72], we have carried out a comparative theoretical study of transition metals and coinage metals. We first used a model of a Ni spheroid with different aspect ratios to calculate the local optical electric field contributing to SERS without taking into account the coupling between particles. The 3D-FDTD result indicates that the Raman signal from a single nanoparticle critically depends on the shape of the nanoparticle and the dielectric constant of the metal as shown in Fig. 4. In order to accurately simulate the detailed nanostructure of nanoparticles, the Yee cell size used in our calculation was set to be $1 \times 1 \times 1\,\text{nm}^3$, which was much smaller than the size of relevant nanoparticle features. The step size of time was set as 1.73 as, and the number of periods of the incident sinusoidal plane wave was set to be 8 to guarantee the calculation convergence, which could be judged by checking whether the near-zone electric field values reach steady state. The amplitude of the sinusoidal plane wave was set to be 1 V/m in the calculation, and the excitation wavelength 632.8 nm.

For a single 60 nm Ni sphere under 632.8 nm excitation, the electric-field enhancement at the tip is just about 4 times the incident optical electric field. Since the SERS enhancement can be estimated by $G = [E_L(\omega_i)/E_{in}(\omega_i)]^2 [E_L(\omega_s)/E_S(\omega_s)]^2$ [68,69], in this case, the SERS enhance-

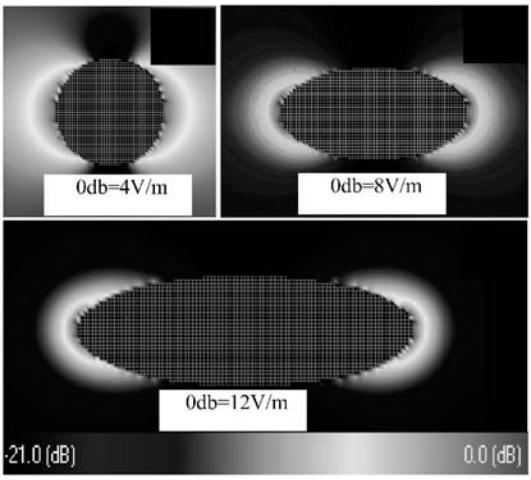

Fig. 4. FDTD simulated electric field distribution of nickel nanospheroid with various aspect ratios, (**a**) 1 : 1, (**b**) 2 : 1, (**c**) 3 : 1. The excitation polarization is along the major axis

ment is about 2.6×10^2. In this approximation, we neglected the influence of the frequency shift of the Raman scattering light on the field enhancement. With the increase of the aspect ratio of the nanoparticle, the maximum *E-field* enhancement increases rapidly. For example, for a spheroid with aspect ratios of 2 : 1 or 3 : 1, the maximum E-field enhancement increases by more than 8 and 12 times, respectively (corresponding to 4×10^3 and 2×10^4 SERS enhancement at the tip, respectively). However, if the aspect ratio of the spheroid becomes 5 : 1 or higher, the maximum electric-field enhancement will decrease slowly. This tendency of the enhancement factor with increasing aspect ratio of the nanoparticle is in agreement with the results of *Schatz* and *Van Duyne* who used electrodynamics corrections to the spheroid model [72]. The above FDTD result is also very close to our previous results using an analytical method for the two-dimensional array model [84].

2.3 3D-FDTD Simulation of the Electromagnetic Field Distribution over a Cauliflower-Like Nanostructure

We found several surfaces with a cauliflower-like morphology, as shown in Fig. 5, to exhibit the highest SERS activity. To explain these experimental observations, the electric-field enhancement of SERS-active Rh systems was estimated by using the 3D-FDTD method. The cauliflower-like nanoparticle was modeled by a 120 nm sphere studded with many 20 nm semispheres, as shown in Fig. 6.

Shown in Fig. 6 is the calculated electric-field distribution on the surface of a Rh sphere with a diameter of 120 nm and covered with 20 nm semi-

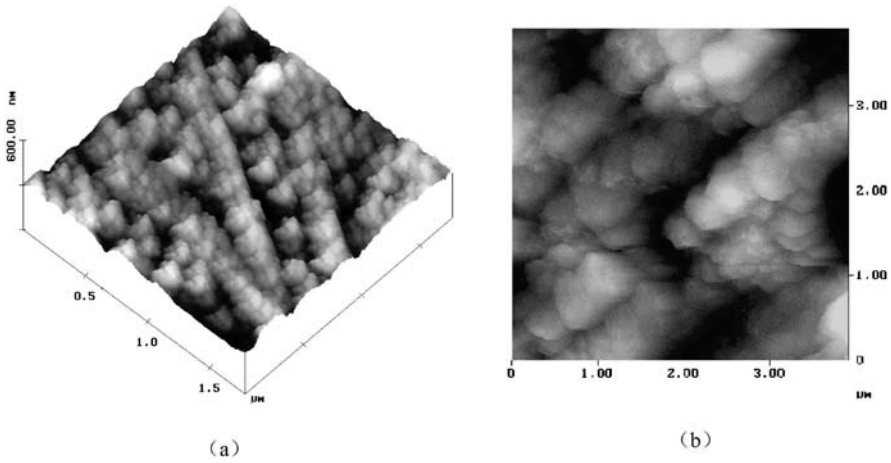

Fig. 5. AFM images of a roughened cauliflower-like Rh electrode (**a**) and a Co electrode (**b**)

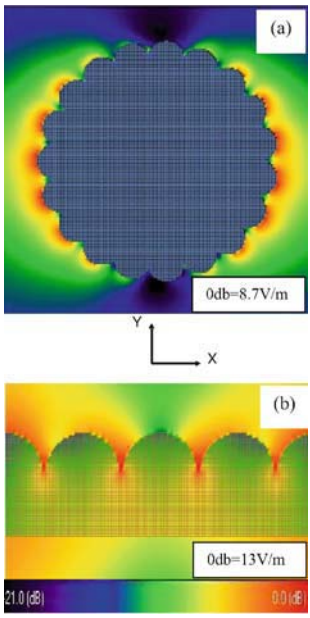

Fig. 6. FDTD simulated electric-field distribution for cauliflower-like Rh nanoparticles. The incident beam illuminates along the y-direction with x-polarization

spherical particles to represent the cauliflower-like nanoparticle (Fig. 6a). It can be seen that the magnitude of the maximally enhanced electric field on the cauliflower nanoparticle is about 8–9 times higher than that of the incident light, and the highest enhancement usually appears at the apex of small semispheres in the "cauliflower". It corresponds to an ca. 6×10^3-fold SERS enhancement on these sites. Note that the magnitude of the maximum electric-field enhancement is just about 4 times larger than the incident light for the smooth sphere under the same excitation condition [60], which means that the maximal enhancement factor for the cauliflower-like nanoparticle is just about 17 times larger than that for the smooth sphere. This different field enhancement could be probably understood on the basis of the lightning-rod effect, which usually results in a relatively large electric-field enhancement near high curvature sites on the surface [76].

It is noted that the field enhancement for the cauliflower-like nanoparticle is not enhanced significantly at the junction point as expected due to the coupling effect between small semispheres. However, if the cauliflower is detached and extended into a plane grating-like structure, the field maximum is shifted to the crevices, as shown in Fig. 6b. The symmetric nature of the nanoparticle may play a role in limiting the electromagnetic modes when the nanostrucutre is coupled with an incident plane wave. Our results seem to indicate that the em enhancement is very sensitive not only to the wavelength and polarization of the exciting light, the electronic property of the metal and the surface morphology, but also to the symmetric nature of the SERS nanostructures.

2.4 3D-FDTD Simulation of the Electromagnetic Field Distribution over a Nanocube Dimer

In our experiment, we found that the SERS activity from Pt nanocubes assembled on a glassy carbon surface is much higher than that from the roughened Pt electrodes. In order to understand this phenomenon, we evaluated the interparticle coupling effects since these Pt nanocube are closely connected to each other at the surface, as can be seen in [60]. When two Pt nanocubes approach each other, the classical electromagnetic theory predicts that a coherent interference of the enhanced field around each particle will result in a dramatic increase in the E-field in the junction between them. Again, the 3D-FDTD method was adopted to simulate the interparticle coupling of Pt nanoparticle dimers.

Figure 7 represents the geometric model in our calculation. On the basis of the TEM image of cubic Pt nanoparticles, the edge length of nanocubes is set to be 20 nm, and the gap between two nanocubes at 1 nm that is just enough to accommodate a layer of molecules. The incident vector is depicted in the figure and the polarization is parallel to the axis along the particle pair (x-axis).

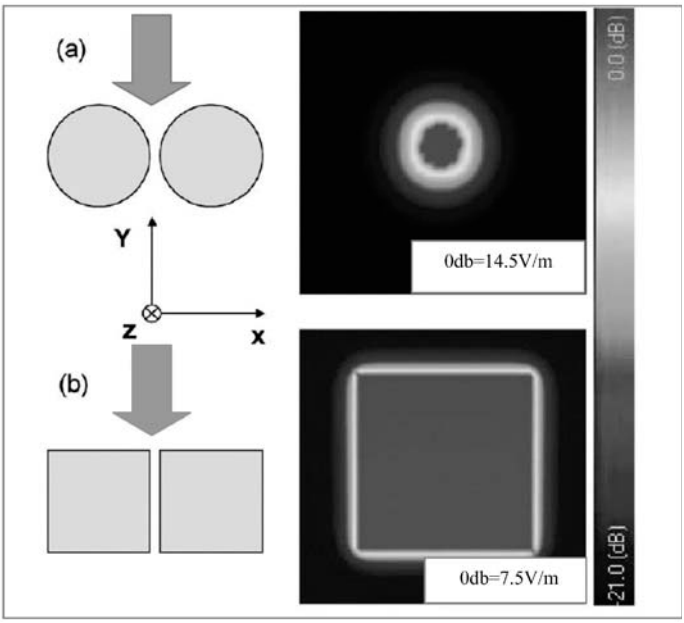

Fig. 7. FDTD simulations of the electric-field distribution in the yz-plane at $x = 0$. The excitation polarization is along the x-axis

It can be seen clearly from the calculation that the electric field reaches the maximum in the gap region in both the sphere (Fig. 7a) and cube models (Fig. 7b). This is in good agreement with the work of *Käll* and coworkers [85] and *Brus* and coworkers [86] that a nanoparticle gap or junction can produce a very large enhancement. The theoretical calculations by *Käll* and coworkers [87, 88] and *Martin* and coworkers [89] can adequately explain the experimental phenomena.

In the present study, the electric-field enhancement is about 14.5 in the gap of the two Pt spheres, while it is about 7.4 in the gap of cubes. This corresponds to SERS enhancement factors of 4.4×10^4 and 3.0×10^3 in the gap for the two shapes, respectively. However, it should be noted that the effective volume in the junction that can offer the largest SERS enhancement is very limited in the case of spheres compared with that of cubes. This fact results in a comparable, even stronger, total SERS signal from nanocubes than from nanospheres.

2.5 3D-FDTD Simulation of Electromagnetic-Field Enhancement of Core-Shell Nanoparticles

To make use of the electromagnetic field enhancement of SERS-active metal to study the non-SERS active overlayers has been a subject of interest for

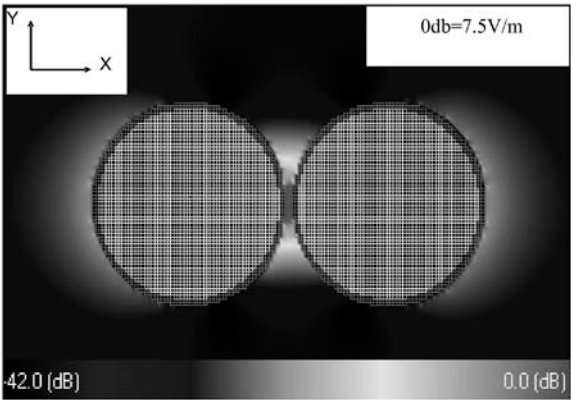

Fig. 8. FDTD simulated electric-field distribution for Au@Pd nanoshell dimers. The excitation polarization is along the x-axis

about 20 years. Recently, we also used the same strategy, however, to prepare Au core Pd shell(Au@Pd) nanoparticles. We found that the SERS activity decays exponentially with increasing shell thickness, which is similar to our previous observation from the Rh layers electrodeposited on a SERS-active Au substrate [90]. The UV-vis data (not shown here) also indicate that the surface-plasmon band of Au is gradually damped with increasing thickness. Most importantly, the highest SERS signal obtained on these Au@Pd nanoparticles can reach up to about 1000 counts per second (cps), which is remarkably higher than that of a roughened Pd electrode (5 cps) and monometallic Pd nanoparticles (60 cps). It clearly demonstrates that a major contribution to the phenomena comes from the long-range effect of the strong electromagnetic field generated by the Au core. To understand the effect of the core, we also simulated the system by the FDTD method.

Figure 8 shows the FDTD-simulated electric-field distribution of the Au@Pd nanoparticle dimers to take account of the coupling effect. In the calculation, the thickness of the Pd shell is set to be 2 nm, the size of the Au core is set to be 55 nm, and the interparticle distance is 1 nm. The 632.8 nm excitation laser is polarized along the axis connecting the two particles. The simulated result shows the maximum electric-field enhancement is also in the junction, which is about 50, corresponding to a SERS enhancement of 6×10^6. It may be necessary to point out the dielectric constants of the shell were directly taken from the bulk value since the large value of the imaginary component of the dielectric constant of transition metals will just result in a relatively small change of the dielectric constant compared with coinage metals in the visible light region. If the thickness is less than 2 nm, the size-dependent effect of the dielectric function of the Pd shell should be taken into account, but we cannot find the necessary parameters, such as the electron mean-free-path for Pd, in the literature. Nevertheless, in our preliminary

calculation, we noticed that the em enhancement increases rapidly with decreasing Pd shell thickness to 1 nm (not shown here) when the bulk dielectric constant was used. The calculation and the experimental data are in good agreement. However, the size-dependent dielectric constants should be used in order to perform more quantitatively simulation on the SERS properties of core-shell nanoparticles when the thickness is around 1 nm.

If the shell thickness exceeds 6 nm, the SERS activity of Au@Pd nanoparticles will show no difference from pure Pd nanoparticles. It should be emphasized here that although the em enhancement is very high in the junction of the nanoshell dimers, the surface-averaged SERS enhancement factor is much lower than 6 orders of magnitude since the number of hottest SERS-active sites, located in the junction, is very limited.

Finally, it may be necessary to note that many molecules and ions adsorb more strongly at transition metals because of the empty d orbital(s) in comparison with the coinage-metals systems. In surface chemistry, most molecules studied can strongly interact with (bind to) the surface and surface chemists cannot ignore the interaction of the surface species with the substrates [13, 91, 92, 93, 94]. It is important for them to describe a clear picture about the molecule–surface interaction, adsorption orientation, surface configuration and coverage, etc. and to find the answer to the phenomenological behavior by analyzing the SERS spectra in much more detail [95, 96]. Therefore, although the electromagnetic effect is the dominant mechanism for most SERS systems, it is necessary, at least for surface chemists, to understand the chemical enhancement, and especially the influence of chemical enhancement on the spectral feature of surface species. Furthermore, when the strong chemical bond is formed, this chemisorption not only changes the electronic structure of the adsorbate itself, but also influences to some extent the surface electronic structure. This may cause the shift of the surface-plasmon resonance frequency and lead to the change of the local electric field at the metal surface [97].

3 SERS From Transition Metals with Ultraviolet Excitation

In all previous SERS studies, light from the visible to the near-infrared region were used for excitation. Extending SERS studies to the UV region may initiate some new approaches. First, it may allow investigation of molecules and nanostructures under new experimental condition including UV-SERS active materials that may or may not be SERS active in the visible or near-infrared region of the em spectrum. Second, since the UV energies are in preresonance or full resonance with electronic absorption of many molecular systems, macromolecules and biomolecules, if some substrates can support the em enhancement in the UV region, the UV laser can excite both the resonance Raman and SERS effect, and the possible applications of surface-enhanced

resonance Raman scattering (UV-SERRS) could be boundless. Moreover, the relevant theoretical approach could provide a deep physical insight into the SERS/SERRS phenomenon. However, many groups including ours have tried but failed to observe SERS from the coinage metals using the ultraviolet (UV) excitation. This is mainly due to the inherent difficulties in generating observable surface enhancement for coinage metals in the UV spectral region, due to the damping of the surface-plasmon resonance by the interband transition absorption when the excitation line is moved to the UV region. Since the optical properties of transition metals are very different from coinage metals, it is worth testing the UV-SERS activity. Recently, we have carried out some preliminary studies using the UV excitation. The results show that UV-SERS can be obtained from a number of adsorbates on different transition-metal surfaces [98, 99].

3.1 Potential-Dependent UV-Raman Spectra from Transition Metals

The surface UV-Raman studies were performed using a He–Cd laser with the wavelength of 325 nm for excitation [98, 99]. Figure 9a shows the potential-dependent spectra of pyridine adsorbed on a roughened Rh electrode surface with a cauliflower-like nanostructure. In the present study, the objective used is of 15× magnification, therefore the interference of the solution signal to the surface signal is quite severe. In order to extract the signal of the surface species, all the surface Raman spectra shown have been subtracted with the corresponding solution spectrum with the intensity of the $933\,\mathrm{cm}^{-1}$ band (total symmetric stretching of ClO_4^-) as an internal reference. As can be seen from Fig. 9a, the frequency and the relative intensity of the major bands of pyridine show a clear potential dependence. The redshift of these bands with the positive movement of the electrode potential is clear evidence of surface species whose surface orientation and coverage are dependent on the applied potential.

Compared with pyridine, SCN^- is a smaller Raman scatterer. However, despite this fact, good-quality spectra were obtained for SCN^- adsorbed on a roughened Rh surface. The experiment was performed with $0.1\,\mathrm{mol}\cdot\mathrm{l}^{-1}$ $NaClO_4$ + $0.01\,\mathrm{mol}\cdot\mathrm{l}^{-1}$ NaSCN solution as the electrolyte, where the ClO_4^- in the solution was again used as the internal reference for subtracting the solution signal. The surface Raman spectra are presented in Fig. 9b, which shows that the intensity of the CN stretching band increases with the negative movement of the electrode potential. In addition, the band frequency redshifts significantly showing an electrochemical Stark effect with a tuning rate of around $73\,\mathrm{cm}^{-1}\cdot\mathrm{V}^{-1}$ of excellent linearity [99].

The good-quality spectra of adsorbed SCN^- can also be observed from Ru and Co electrode surfaces [98, 99] as well as Pt nanocube-on-electrodes [100]. The potential-dependent spectra of the adsorbed SCN^- on a Ru-coated glassy carbon electrode and on a roughened Co massive electrode are shown in

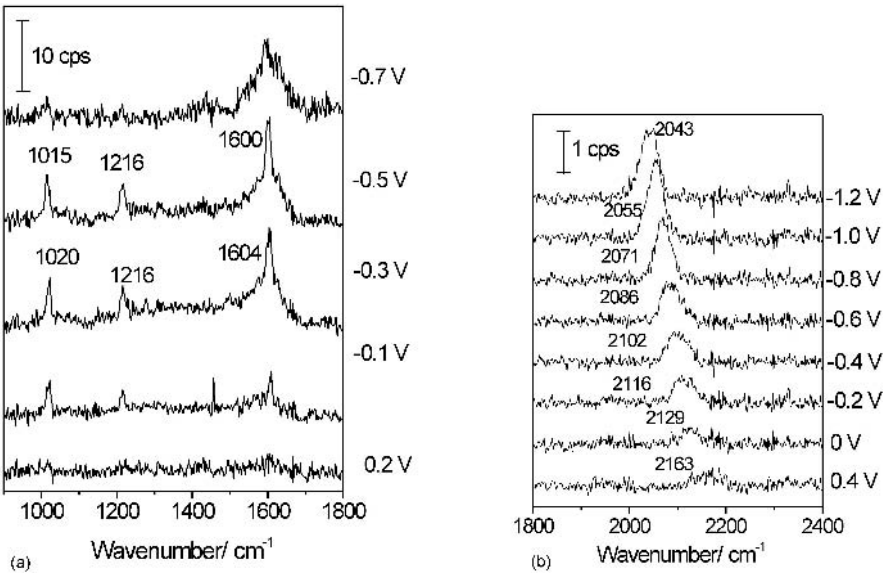

Fig. 9. (**a**) UV-SER spectra of pyridine adsorbed on a Rh electrode at different potentials; (**b**) UV-SER spectra of SCN^- adsorbed on a roughened Rh electrode in $0.1\,\mathrm{mol}\cdot\mathrm{l}^{-1}$ $NaClO_4$ + $0.01\,\mathrm{mol}\cdot\mathrm{l}^{-1}$ NaSCN at different potentials. Excitation line: 325 nm

Figs. 10a and 10b. On these two electrodes, only one peak was observed in the negative potential region and the v_{CN} blueshifts with the positive movement of the potential. Another peak appears at the high-frequency side of the original peak from -0.1 V for Ru electrode and -0.5 V for Co electrode, indicating that there is another type of surface SCN^- species in the positive-potential region.

It may be necessary to note that photodecomposition on the surface is often observed and it may limit to some extent the application of UV-SERS. However, the successful observation of a surface UV-Raman signal from adsorbed species indicates a promising future for this approach. Furthermore, according to our calibration, the signal of silicon ($520.6\,\mathrm{cm}^{-1}$) obtained on the visible Raman system is about 40-fold higher than that on the UV-Raman system. This is almost opposite to that predicted by theory if we consider the fourth-power-law relationship of Raman intensity with that of the incident laser frequency. This situation makes the UV-Raman technique very promising since we still have a great chance to improve significantly the detection sensitivity of the UV-Raman instrument.

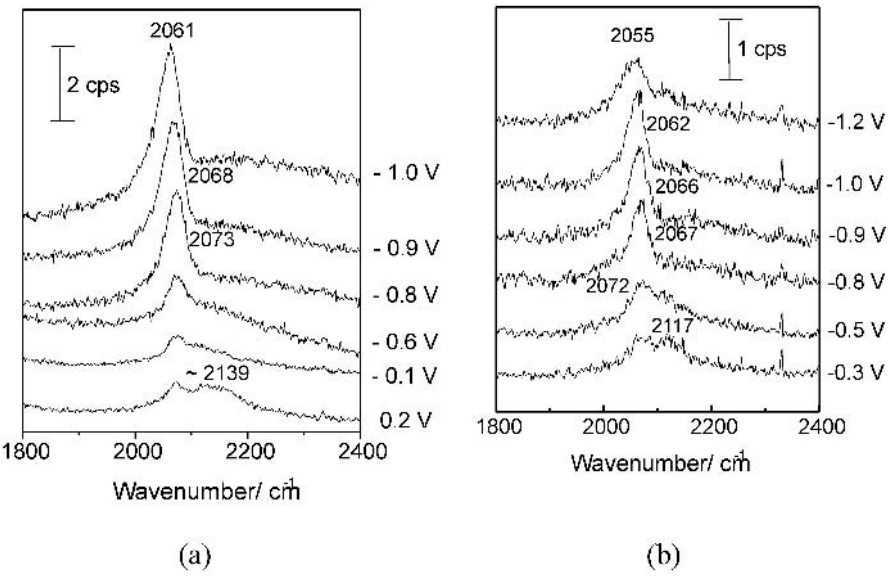

Fig. 10. UV-SER spectra SCN^- adsorbed on a Ru-coated glass carbon electrode (**a**) and on a Co electrode (**b**) in $0.1\,\mathrm{mol}\cdot\mathrm{l}^{-1}$ $NaClO_4$ + $0.01\,\mathrm{mol}\cdot\mathrm{l}^{-1}$ NaSCN at different potentials. Excitation line: 325 nm, acquisition time: 200 s

3.2 Confirmation of UV-SERS Effect on Transition Metals

It can be seen that the UV-Raman signal of SCN^- on the Ru coated glassy carbon electrode is stronger than that on the roughened Rh and Co surfaces. This may indicate the importance of proper matching of the incident light frequency with that of the optical properties of the surface nanostructures. It is necessary to clarify if there is the SERS effect with ultraviolet excitation and whether transition metals can exhibit UV-SERS activity. We performed a similar calculating method mentioned above and also considering the special feature of the UV Raman microscope [99]. From the experimental results shown in Fig. 9a, the surface enhancement factor for the adsorbed SCN^- is calculated to be about 345, indicating that the surface enhancement factor of the Rh surface in the UV regions is at least 2 orders of magnitude. It should be pointed out that although this value is considerably lower compared with that of coinage metals in the visible region, it is indeed meaningful for studying the adsorbed surface species with UV excitation.

It is of special interest to work out why transition metal and not the typical SERS metals support SERS activity in the UV region. We performed a preliminarily theoretical calculation of the wavelength-dependent surface enhancement factor for Rh and Ag using the method described by *Zeman* and *Schatz* [101], based on the em model. The Rh and Ag surfaces were simulated with a Rh and a Ag ellipsoidal nanoparticles with 3 : 1 aspect ratio (semi-

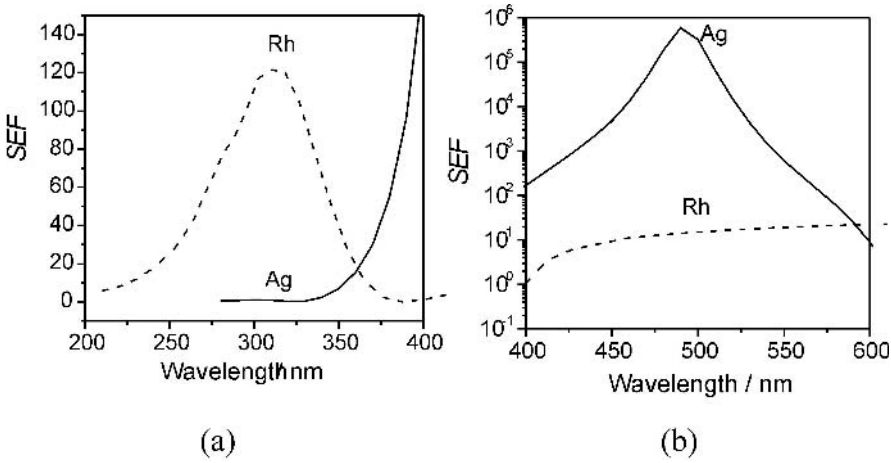

Fig. 11. Averaged enhancement factors for Ag and Rh ellipsoids with the aspect ratio of 3 : 1 in the UV spectral region (**a**) and the visible region (**b**) of the em spectrum

major axis $a = 45$ nm and semiminor axis $b = 15$ nm), respectively. As is well known, the field at the tip of the ellipsoid is much stronger than the other region of the particles when the electric-field vector of the incident light is polarized along the major axis. However, in a real SERS experiment, the signal is an average of the signal from all over the particle's surface. Therefore, only the averaged enhancement is meaningful for comparing experimental and theoretical results. The calculated averaged surface enhancement factors at different wavelengths for the above two systems are shown in Fig. 11. The averaged G for Ag in the visible region can be as high as 10^6, contributed by both surface-plasmon resonance and the lightning-rod effect. However, it decreases sharply when the excitation wavelength is moved into the UV spectral region and there is essentially no enhancement when the wavelength is shorter than 325 nm because this condition is then not appropriate to induce surface-plasmon resonance. The real dielectric constant of Ag is changed from the suitable negative value at about -10 at around 500 nm to the positive value of about 0.5 at around 325 nm. Accordingly, it seems to be easy to understand the diminishment of the enhancement in the UV region for Ag. In contrast, the G value of a Rh ellipsoidal does not change so significantly as wavelength varies in the visible region, but shows a small peak with a maximum of ca. 10^2 at around 325 nm. The real dielectric constant of Rh is changed from -18 at around 500 nm to about -10 at around 325 nm.

This preliminary theoretical calculation infers that some transition metals, rather than the typical SERS metals, may have relatively suitable optical properties to present observable SERS signal in the UV region. Although a more systematic study is required, our preliminary approach of UV-SERS not

only demonstrates the importance of optical properties of the substrate in UV-SERS, but also provides some useful information on the physics behind SERS.

4 Conclusion

In this Chapter, we employed the 3D-FDTD method to calculate and evaluate the local electromagnetic field by investigating the effect of the surface geometry, the size, shape, and aggregation forms of nanoparticles on the SERS activity of transition metal systems. Our calculation on the cauliflower-structured nanoparticles shows that the em enhancement is sensitive not only to the polarization of the exciting light, the electronic property of metal and the surface morphology, but also to the symmetric nature of the SERS nanostructures. We demonstrated that the reason for the high enhancement in the nanocube system could be due to the large effective volume involved in the strong coupling between neighboring nanocubes. For the core-shell system, we show that the em enhancement decreases rapidly with increasing shell thickness and when the shell thickness exceeds 6 nm, the core no longer influences the SERS of the shell. The detection of a reasonably good UV-SERS signal on Pt, Rh, Ru and Co surfaces rather than Ag and Au is mainly due to the intrinsically suitable optical properties of transition metals in the UV region. Overall, the extension of SERS substrate to the transition-metal systems and use of UV excitation have improved the generality of the SERS technique and could be helpful for comprehensive understanding of SERS.

References

[1] Z. Q. Tian: Special issue on SERS, J. Raman Spectrosc. **36** (2005)
[2] A. Campion, P. Kambhampati: Chem. Soc. Rev. **27**, 241 (1998)
[3] K. Kneipp, H. Kneipp, I. Itzkan, R. R. Dasari, M. S. Feld: Chem. Rev. **99**, 780 (1999)
[4] M. Moskovits, L. L. Tay, J. Yang, T. Haslett: SERS and the single molecule, in V. Shalaev (Ed.): *Optical Properties of Nanostructured Random Media* (Springer, Berlin, Heidelberg, New York 2002) pp. 215–226
[5] K. L. Kelly, E. Coronado, L. L. Zhao, G. C. Schatz: J. Phys. Chem. B **107**, 668 (2003)
[6] J. Jiang, K. Bosnick, M. Maillard, L. Brus: J. Phys. Chem. B **107**, 9964 (2003)
[7] T. R. Jensen, M. D. Malinsky, C. L. Haynes, R. P. Van Duyne: J. Phys. Chem. B **104**, 10549 (2000)
[8] S. M. Nie, R. N. Zare: Ann. Rev. Biophys. Biomol. Struct. **26**, 567 (1997)
[9] Z. Q. Tian, B. Ren: Ann. Rev. Phys. Chem. **55**, 197 (2004)
[10] R. A. Lund, R. R. Smardzewski, R. E. Tevault: J. Chem. Phys. **88**, 1731 (1984)

[11] W. Schulze, K. P. Charle, U. Kloss: Surf. Sci. **156**, 822 (1985)
[12] D. P. DiLella, J. S. Suh, M. Moskovits: *Proceedings of the* 8^{th} *International Conference on Raman Spectroscopy* (Wiley, Chichester, UK 1982) p. 63
[13] Z. Q. Tian, B. Ren, D. Y. Wu: J. Phys. Chem. B **106**, 9463 (2002)
[14] R. P. Van Duyne, J. P. Haushalter: J. Phys. Chem. **87**, 2999 (1983)
[15] J. C. Rubim, G. Kannen, D. Schumacher, J. Dunnwald, A. Otto: Appl. Surf. Sci. **37**, 233 (1989)
[16] M. Fleischmann, Z. Q. Tian: J. Electroanal. Chem. **217**, 385 (1987)
[17] M. Fleischmann, Z. Q. Tian, L. J. Li: J. Electroanal. Chem. **217**, 397 (1987)
[18] G. Mengoli, M. M. Musiani, M. Fleischmann, B. W. Mao, Z. Q. Tian: Electrochem. Acta **32**, 1239 (1987)
[19] L. W. H. Leung, M. J. Weaver: J. Am. Chem. Soc. **109**, 5113 (1987)
[20] L. W. H. Leung, M. J. Weaver: J. Electroanal. Chem. **217**, 367 (1987)
[21] Y. Zhang, X. Gao, M. J. Weaver: J. Phys. Chem. **97**, 8656 (1993)
[22] S. Zou, M. J. Weaver: Anal. Chem. **70**, 2387 (1998)
[23] S. Zou, C. T. Williams, E. K. Y. Chen, M. J. Weaver: J. Am. Chem. Soc. **120**, 3811 (1998)
[24] M. J. Weaver, S. Zou, H. Y. H. Chan: Anal. Chem. **72**, 38 A (2000)
[25] M. F. Mrozek, Y. Xie, M. J. Weaver: Anal. Chem. **73**, 5953 (2001)
[26] C. A. Melendres, M. Pankuch, Y. S. Li, R. L. Knight: Electrochim. Acta **37**, 2747 (1992)
[27] C. J. Zhong, Z. Q. Tian, Z. W. Tian: Sci. China B **33**, 656 (1990)
[28] G. Xue, Y. Lu, G. Shi: Polym. **35**, 2488 (1994)
[29] C. J. L. Constantino, T. Lemma, P. A. Antunes, R. Aroca: Anal. Chem. **73**, 3674 (2001)
[30] R. F. Aroca, C. J. L. Constantino: Langmuir **16**, 5425 (2000)
[31] C. A. Melendres, N. Camillone, T. Tipton: Electrochim. Acta **34**, 281 (1989)
[32] C. A. Melendres: *Spectroscopic and Diffraction Techniques in Interfacial Electrochemistry* (Kluwer Academic, Dordrecht 1990) p. 181
[33] R. P. Cooney, M. Fleischmann, P. J. Hendra: J. Chem. Soc. Chem. Commun. **7**, 235 (1977)
[34] M. Fleischmann, D. Sockalingum, M. M. Musiani: Spectrochim. Acta **46A**, 285 (1990)
[35] C. Jennings, R. Aroca, A. M. Hor, R. O. Loutfy: Anal. Chem. **56**, 2033 (1984)
[36] R. Aroca, C. Jennings, G. J. Kovacs, R. O. Loutfy, P. S. Vincett: J. Phys. Chem. **89**, 4051 (1985)
[37] T. Maeda, Y. Sasaki, C. Horie, M. Osawa: J. Electron. Spectrosc. Relat. Phenom. **64/65**, 381 (1993)
[38] S. A. Bilmes, J. C. Rubim, A. Otto, A. J. Arvia: Chem. Phys. Lett. **159**, 89 (1989)
[39] S. A. Bilmes: Chem. Phys. Lett. **171**, 141 (1990)
[40] C. Shannon, A. Campion: J. Phys. Chem. **92**, 1385 (1988)
[41] L. Guo, Q. J. Huang, X. Y. Li, S. H. Yang: Phys. Chem. Chem. Phys. **3**, 1661 (2001)
[42] H. Yamada, Y. Yamamoto: Chem. Phys. Lett. **77**, 520 (1981)
[43] H. Yamada, Y. Yamamoto: Surf. Sci. **134**, 71 (1983)
[44] M. P. Cline, P. W. Barber, R. K. Chang: J. Opt. Soc. Am. B **3**, 15 (1986)
[45] B. J. Messinger, K. U. von Raben, R. K. Chang, P. W. Barber: Phys. Rev. B **24**, 649 (1981)

[46] Z. Q. Tian, B. Ren, B. W. Mao: J. Phys. Chem. B **101**, 1338 (1997)
[47] Z. Q. Tian, J. S. Gao, X. Q. Li, B. Ren, Q. J. Huang, W. B. Cai, F. M. Liu, B. W. Mao: J. Raman Spectrosc. **29**, 703 (1998)
[48] W. B. Cai, B. Ren, X. Q. Li, C. X. She, F. M. Liu, X. W. Cai, Z. Q. Tian: Surf. Sci. **406**, 9 (1998)
[49] Q. J. Huang, X. Q. Li, J. L. Yao, B. Ren, W. B. Cai, J. S. Gao, B. W. Mao, Z. Q. Tian: Surf. Sci. **427/428**, 162 (1999)
[50] B. Ren, Q. J. Huang, W. B. Cai, B. W. Mao, F. M. Liu, Z. Q. Tian: J. Electroanal. Chem. **415**, 175 (1996)
[51] J. S. Gao, Z. Q. Tian: Spectrochim. Acta A **53**, 1595 (1997)
[52] Q. J. Huang, J. L. Yao, R. A. Gu, Z. Q. Tian: Chem. Phys. Lett. **271**, 101 (1997)
[53] P. G. Cao, J. L. Yao, B. Ren, B. W. Mao, R. A. Gu, Z. Q. Tian: Chem. Phys. Lett. **316**, 1 (2000)
[54] D. Y. Wu, Y. Xie, B. Ren, J. W. Yan, B. W. Mao, Z. Q. Tian: Phys. Chem. Comm. **18**, 1 (2001)
[55] B. Chase: Appl. Spectrosc. **48**, 14 A (1994)
[56] Z. Q. Tian, B. Ren: *Encyclopedia of Analytical Chemistry* (Wiley, New York 2000) p. 9162
[57] B. Ren, X. F. Lin, J. W. Yan, B. W. Mao, Z. Q. Tian: J. Phys. Chem. B **107**, 899 (2003)
[58] J. L. Yao, J. Tang, D. Y. Wu, D. M. Sun, K. H. Xue, B. Ren, B. W. Mao, Z. Q. Tian: Surf. Sci. **514**, 108 (2002)
[59] J. L. Yao, G. P. Pan, K. H. Xue, D. Y. Wu, B. Ren, D. M. Sun, J. Tang, X. Xu, Z. Q. Tian: Pure Appl. Chem. **72**, 221 (2000)
[60] Z. Q. Tian, Z. L. Yang, B. Ren, J. F. Li, Y. Zhang, X. F. Lin, J. W. Hu, D. Y. Wu: Faraday Discuss. **132**, 159 (2006)
[61] X. Xu, B. Ren, D. Y. Wu, H. Xian, X. Lu, P. Shi, Z. Q. Tian: Surf. Interf. Anal. **28**, 111 (1999)
[62] X. Xu, D. Y. Wu, B. Ren, H. Xian, Z. Q. Tian: Chem. Phys. Lett. **311**, 193 (1999)
[63] S. Z. Zou, C. T. Williams, E. K. Y. Chen, M. J. Weaver: J. Am. Chem. Soc. **120**, 3811 (1998)
[64] M. J. Weaver: Top. Catal. **8**, 65 (1999)
[65] V. M. Browne, S. G. Fox, P. Hollins: Catal. Today **9**, 1 (1991)
[66] B. Ren, X. Q. Li, C. X. She, D. Y. Wu, Z. Q. Tian: Electrochim. Acta **46**, 193 (2000)
[67] R. K. Chang, T. E. Furtak: *Surface Enhanced Raman Scattering* (Plenum, New York 1982)
[68] A. Otto: Surface-enhanced Raman-scattering – Classical and chemical origins, in M. Cardona, G. Guntherodt (Eds.): *Light Scattering in Solids* (Springer, Berlin 1984) pp. 289–418
[69] M. Kerker: Acct. Chem. Res. **17**, 271 (1984)
[70] H. Metiu, P. Das: Annu. Rev. Phys. Chem. **35**, 507 (1984)
[71] M. Moskovits: Rev. Mod. Phys. **57**, 783 (1985)
[72] G. C. Schatz, R. P. Van Duyne: *Handbook of Vibrational Spectroscopy* (Wiley, Chichester 2002) pp. 759–774
[73] H. Ebert: Rep. Prog. Phys. **59**, 1665 (1996)
[74] J. H. Weaver: Phys. Rev. B **11**, 1416 (1975)

[75] M. A. Ordal, R. J. Bell, R. W. Alexander, L. L. Long, M. R. Querry: Appl. Opt. **24**, 4493 (1985)
[76] J. Gersten, A. Nitzan: J. Chem. Phys. **73**, 3023 (1980)
[77] P. B. Johnson, R. W. Christy: Phys. Rev. B **6**, 4370 (1972)
[78] E. D. Palik: *Handbook of Optical Constants of Solids* (Academic, New York 1985)
[79] L. C. Chu, S. Wang: Phys. Rev. B **31**, 693 (1985)
[80] E. Hao, G. C. Schatz: J. Chem. Phys. **120**, 357 (2004)
[81] P. W. Barber, S. C. Hill: *Light Scattering by Particles: Computational Methods* (World Scientific, Singapore 1990)
[82] K. S. Kunz, R. J. Luebbers: *The Finite Difference Time Domain Method for Electromagnetics* (CRC and LLC, Boca Raton 1993)
[83] J. T. Krug II, E. J. Sanchez, X. S. Xie: J. Chem. Phys. **116**, 10895 (2002)
[84] Z. L. Yang, D. Y. Wu, J. L. Yao, J. Q. Hu, B. Ren, H. G. Zhou, Z. Q. Tian: Chin. Sci. Bull. **47**, 1983 (2002)
[85] H. X. Xu, E. J. Bjerneld, M. Käll, L. Borjesson: Phys. Rev. Lett. **83**, 4357 (1999)
[86] M. Michaels, M. Nirmal, L. E. Brus: J. Am. Chem. Soc. **121**, 9932 (1999)
[87] H. X. Xu, J. Aizpurua, M. Käll, P. Apell: Phys. Rev. E **62**, 4318 (2000)
[88] H. X. Xu, M. Käll: Phys. Rev. Lett. **89**, 246802 (2002)
[89] J. P. Kottmann, O. J. F. Martin, D. R. Smith, S. Schultz: Phys. Rev. B **64**, 235402 (2001)
[90] S. Zou, M. J. Weaver, X. Q. Li, B. Ren, Z. Q. Tian: J. Phys. Chem. B **103**, 4218 (1999)
[91] A. Otto, I. Mrozek, H. Grabhorn, W. Akemann: J. Phys. Condens. Matter **4**, 1143 (1992)
[92] D. Y. Wu, B. Ren, Y. X. Jiang, X. Xu, Z. Q. Tian: J. Phys. Chem. A **106**, 9042 (2002)
[93] D. Y. Wu, B. Ren, X. Xu, G. K. Liu, Z. L. Yang, Z. Q. Tian: J. Chem. Phys. **119**, 1701 (2003)
[94] D. Y. Wu, M. Hayashi, S. H. Lin, Z. Q. Tian: Spectrochim. Acta A **60**, 137 (2004)
[95] J. Billman, A. Otto: Surf. Sci. **138**, 1 (1984)
[96] J. F. Arenas, I. L. Tocon, J. C. Otero, J. I. Marcos: J. Phys. Chem. **100**, 9254 (1996)
[97] M. D. Malinsky, K. L. Kelly, G. C. Schatz, R. P. Van Duyne: J. Am. Chem. Soc. B **123**, 1471 (2001)
[98] B. Ren, X. F. Lin, Z. L. Yang, R. F. Aroca, B. W. Mao, Z. Q. Tian: J. Am. Chem. Soc. **125**, 9598 (2003)
[99] X. F. Lin, B. Ren, Z. L. Yang, G. K. Liu, Z. Q. Tian: J. Raman Spectrosc. **36**, 606 (2005)
[100] L. Cui, Y. Zhang, Z. L. Yang, B. Ren, Z. Q. Tian: in preparation
[101] E. J. Zeman, G. C. Schatz: J. Phys. Chem. **91**, 634 (1987)

Index